

Supplementary Material: Characteristics and Applications of Current-Driven Magnetic Skyrmion Strings

Zhao-Nian Jin(金兆年)¹, Min-Hang Song(宋敏航)², He-Nan Fang(方贺男)², Lin Chen(陈琳)²,

Jiang-Wei Chen(陈将伟)², and Zhi-Kuo Tao(陶志阔)^{2*}

¹Bell Honors School, Nanjing University of Posts and Telecommunications, Nanjing 210003, China

²College of Electronic and Optical Engineering & College of Microelectronics,
Nanjing University of Posts and Telecommunications, Nanjing 210003, China

* Corresponding author. Email: zktao@njupt.edu.cn

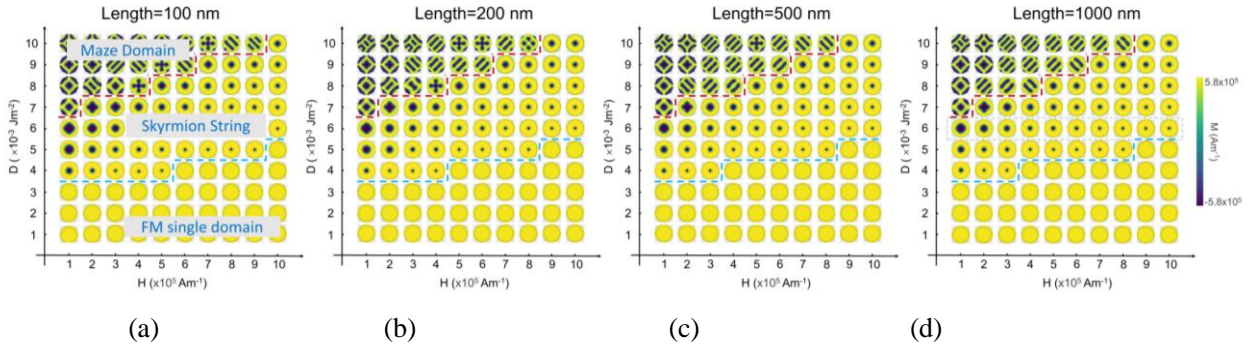


Fig. S1 Phase diagrams for skyrmion string formation as a function of D and H with lengths of (a) 100 nm, (b) 200 nm, (c) 500 nm, and (d) 1000 nm. We can see that the lower value of D is unfavorable for skyrmion string generation. In the following simulation of skyrmion strings, the external applied magnetic field is set to $5 \times 10^5 \text{ Am}^{-1}$, and DMI constant D is set to $6.0 \times 10^{-3} \text{ Jm}^{-2}$. Although the D value is larger than the usual experimental data, a distinct varying morphology or configuration with a wider range of external field H can be achieved when the D value is set to $6 \times 10^{-3} \text{ Jm}^{-2}$ as shown in all four conditions in Fig. S1.

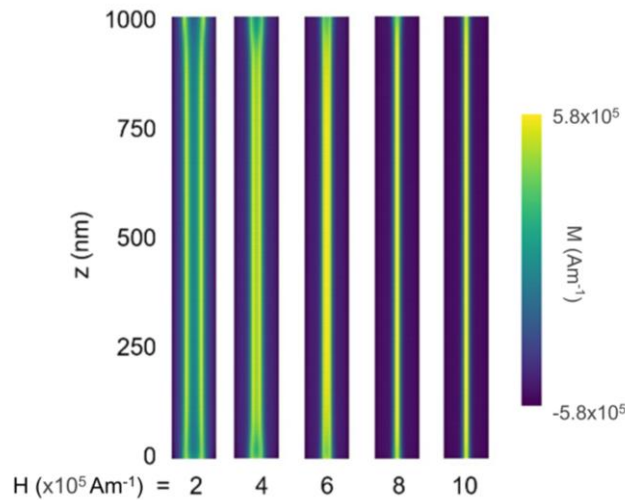


Fig. S2 Cross-section views of skyrmion string with H changing from $2 \times 10^5 \text{ Am}^{-1}$ to $10 \times 10^5 \text{ Am}^{-1}$. The 2D skyrmions at different z -axis locations present slightly different profiles.

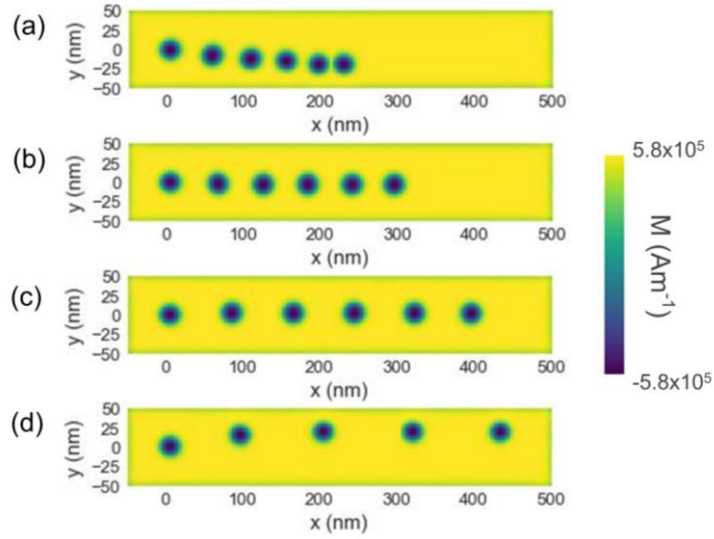


Fig. S3 The moving profiles with ζ of (a) 0.2, (b) 0.3, (c) 0.4 and (d) 0.6 under $j=3.84 \times 10^7 \text{ Am}^{-2}$.

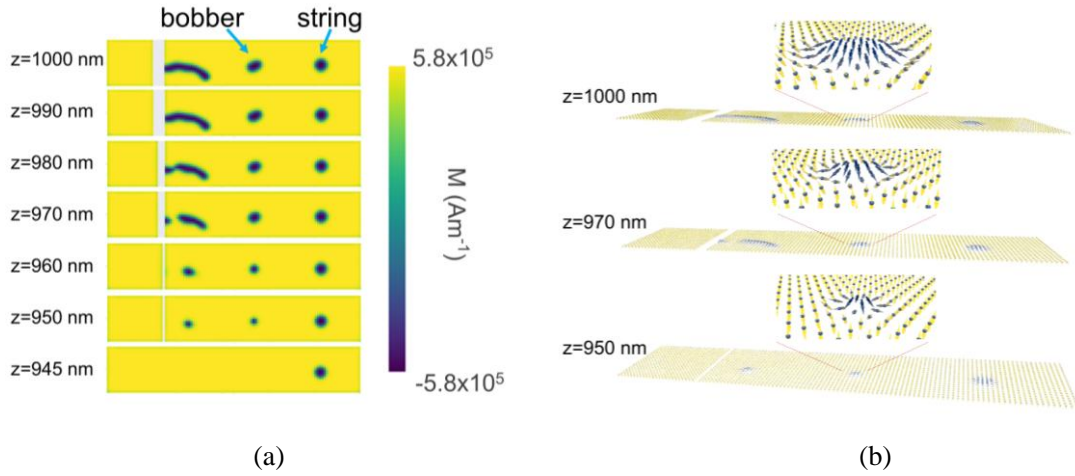


Fig. S4 (a) Plane views of bobber generation process in driving times of 0.5 ns with $j=3.84 \times 10^8 \text{ Am}^{-2}$. (b) 3D views of the bobber with the magnetic vector field.

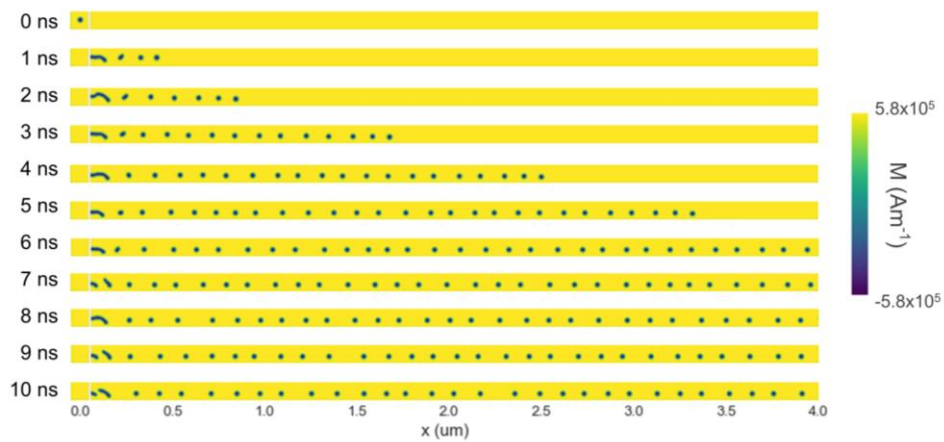
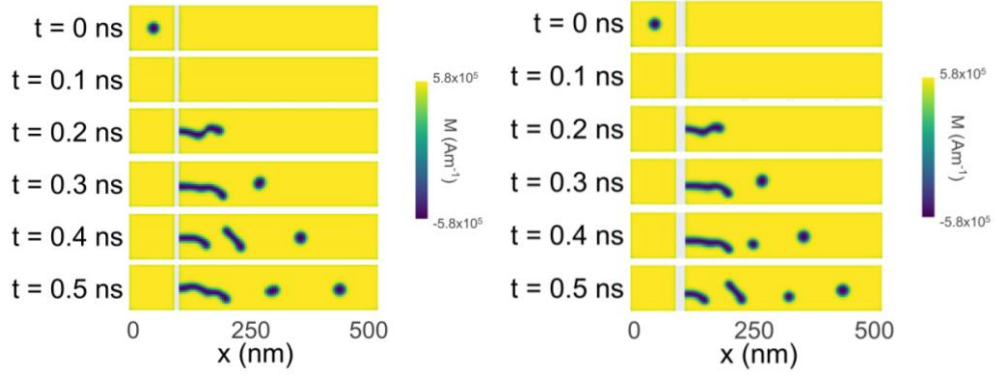
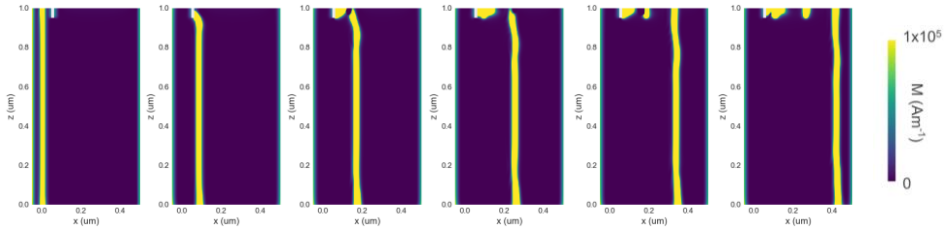


Fig. S5 Surface views of the skyrmion strings and bobbles in driving times of 10 ns with $j=3.84 \times 10^8 \text{ Am}^{-2}$ and $\zeta=\alpha=0.3$.

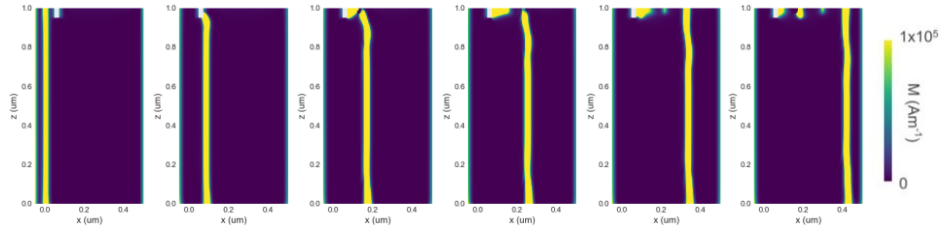


(a)

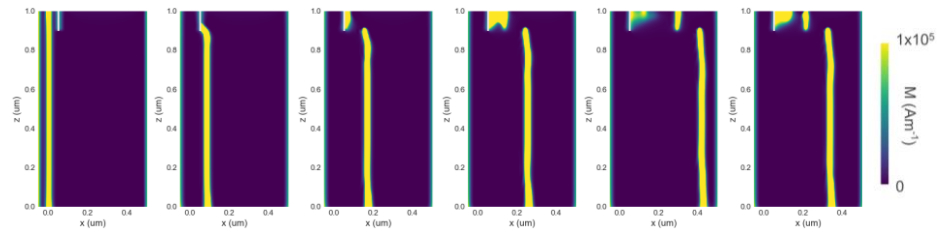
(b)



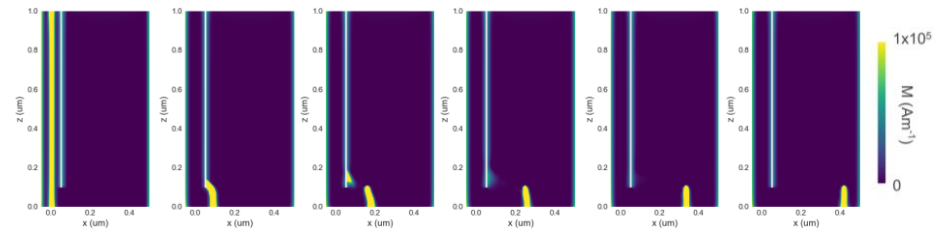
(c)



(d)



(e)



(f)

Fig. S6 Surface views and cross-section views of the skyrmion strings and bobbles in driving times of 0.5 ns with $j=3.84 \times 10^8 \text{ Am}^{-2}$ for $h=50 \text{ nm}$ and (a, c) $l=10 \text{ nm}$ and (b, d) $l=20 \text{ nm}$. The bobbles can be generated stably. When l is fixed at 5 nm and h becomes larger (100nm in (e) and 900 nm in (f)), there are no bobbles generated.

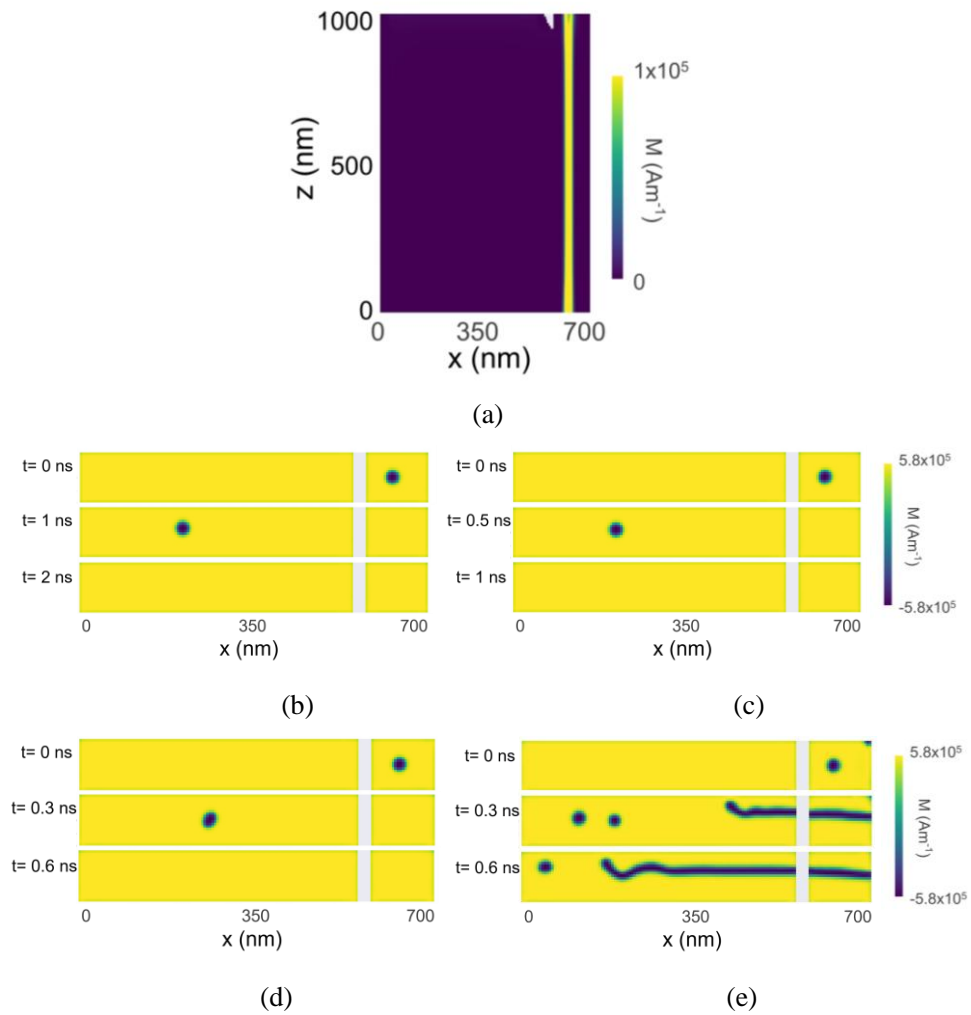
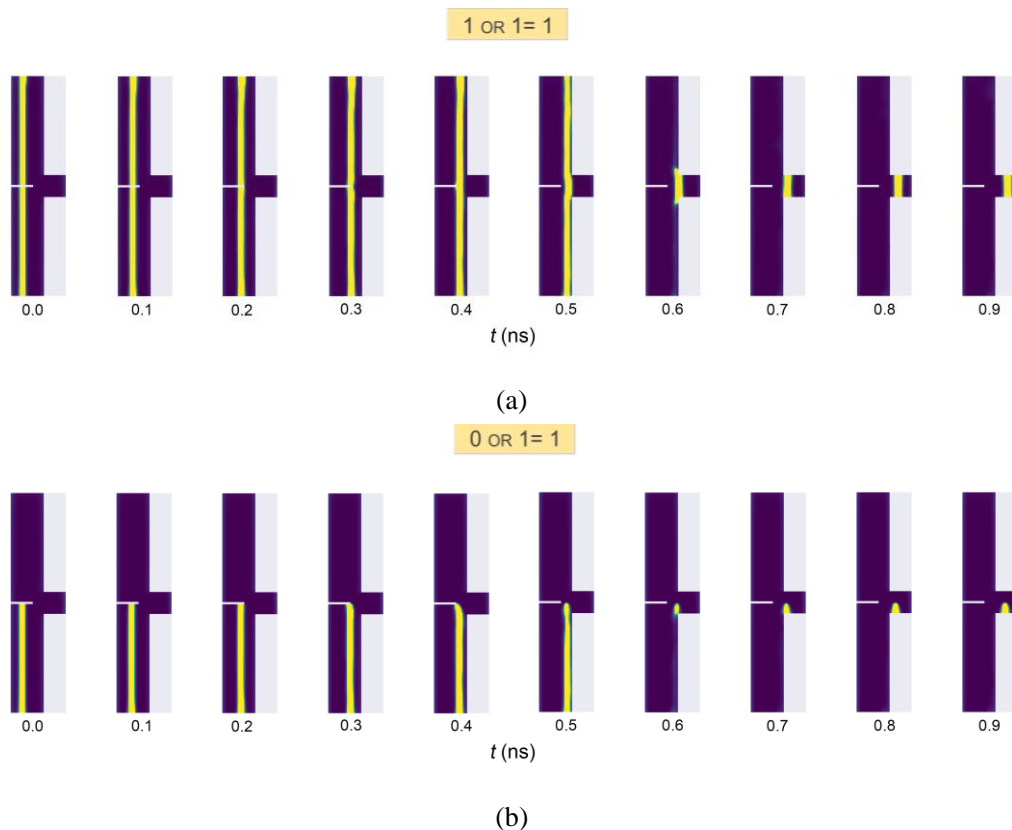
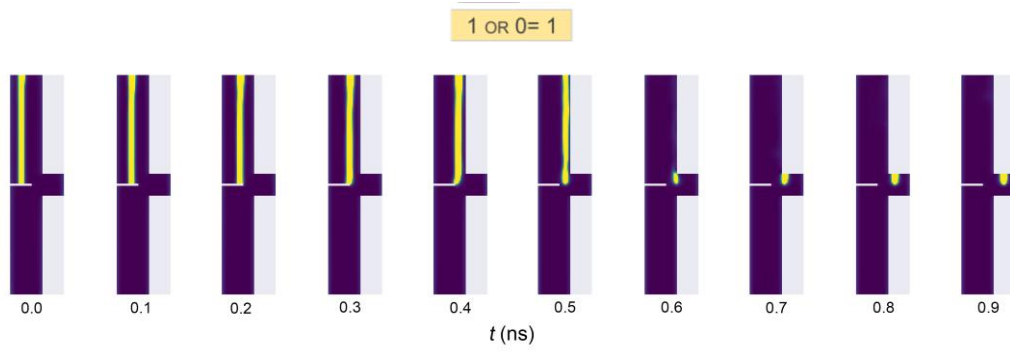
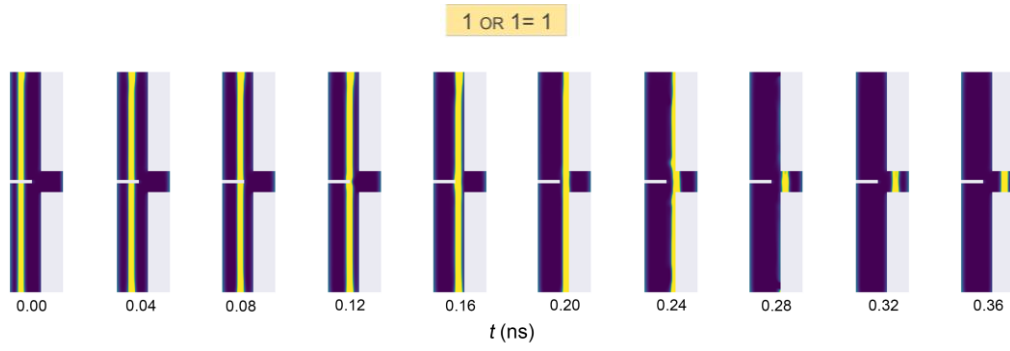


Fig. S7 (a) The simulation scheme when the biased driving current is reversed. The current is (b) $-1.92 \times 10^8 \text{ Am}^{-2}$, (c) $-3.84 \times 10^8 \text{ Am}^{-2}$, (d) $-5.76 \times 10^8 \text{ Am}^{-2}$ and (e) $-7.68 \times 10^8 \text{ Am}^{-2}$ respectively. No generated stable bobbars can be detected when the driving current moves from right to left with any current density.

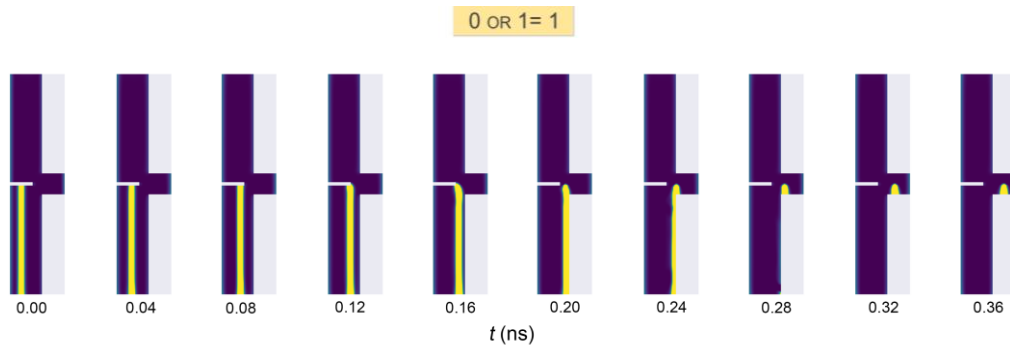




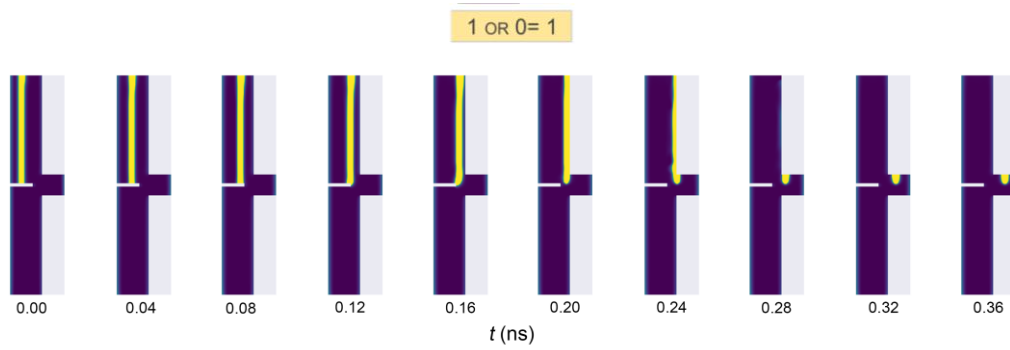
(c)



(d)



(e)



(f)

Fig. S8 OR gate realized through current-driven skyrmion strings with j of $7.68 \times 10^7 \text{ Am}^{-2}$ and $1.92 \times 10^8 \text{ Am}^{-2}$, respectively.

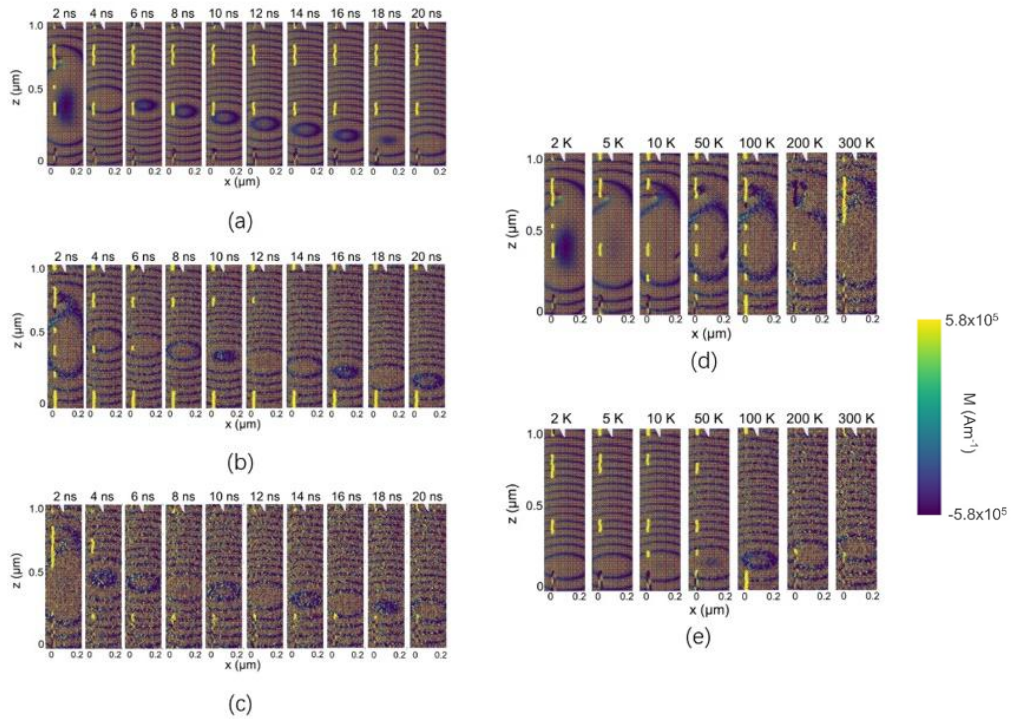


Fig. S9 Cross-section views of skyrmion strings in 20 ns at temperature (a) $T=2$ K, (b) $T=100$ K, and (c) $T=300$ K. Cross-section views of skyrmion strings at temperatures ranging from 2 K to 300 K at simulation time (d) $t=0$ ns and (e) $t=20$ ns.